

# Effect of the chiral chemical potential on the position of the critical endpoint

Bin Wang,<sup>1,2,\*</sup> Yong-Long Wang,<sup>3,4</sup> Zhu-Fang Cui,<sup>3,6</sup> and Hong-Shi Zong<sup>3,5,6,†</sup>

<sup>1</sup>Key Laboratory of Modern Acoustics, MOE, Institute of Acoustics, and Department of Physics, Nanjing University, Nanjing 210093, China

<sup>2</sup>Department of Physics, Huazhong University of Science and Technology, Wuhan 430074, China

<sup>3</sup>Department of Physics, Nanjing University, Nanjing 210093, China

<sup>4</sup>Department of Physics, School of Science, Linyi University, Linyi 276005, China

<sup>5</sup>Joint Center for Particle, Nuclear Physics and Cosmology, Nanjing 210093, China

<sup>6</sup>State Key Laboratory of Theoretical Physics, Institute of Theoretical Physics, CAS, Beijing 100190, China  
(Received 20 November 2013; published 19 February 2015)

The effect of chiral imbalance on the QCD phase structure is studied in a framework of Dyson–Schwinger equations. It is found that the chiral phase transition is always a crossover in the  $T - \mu_5$  plane when  $\mu$  is 0 MeV or small values. The trail of the critical endpoints (CEPs) along with the variation of the chiral chemical potential is given. We find that the effect of  $\mu_5$  is somewhat different from the existing chiral model calculations; namely, the CEP first moves roughly along the phase boundary of  $T - \mu$  plane in a smaller  $\mu$  direction, as in the chiral model calculations, but turns in the opposite direction to move away from the small chemical potential region, which has never been observed before. In addition, we also discuss the possibility of whether the study at finite temperature and chiral chemical potential can provide some useful information for the detection of the CEP at finite temperature and baryon chemical potential, since the former can be calculated in lattice QCD without the sign problem.

DOI: 10.1103/PhysRevD.91.034017

PACS numbers: 25.75.Nq, 12.38.Aw, 12.38.Mh

## I. INTRODUCTION

It is well known that a pure non-Abelian gauge theory has many vacua characterized by different integer Chern–Simons numbers. These different vacua can be twisted from one to another by sphalerons or instantons, which are the gluon configurations associated with nonzero winding numbers [1,2]

$$Q_W = \frac{g^2}{32\pi^2} \int d^4x \epsilon_{\mu\nu\rho\omega} F_a^{\mu\nu} F^{a\rho\omega}. \quad (1)$$

At high temperature, copious sphalerons can be created [3,4], and through the Adler–Bell–Jackiw relation [5–7], the quarks that interact with these gluon configurations would acquire chirality, i.e., the chiral imbalance

$$N_5 = N_R - N_L = n_5 V = 2N_f Q_W. \quad (2)$$

Because there is no direct  $P$  and  $CP$  violation in QCD, it has the equal probability to produce a sphaleron with either a positive or negative winding number. So, the chirality in each event of quark-gluon plasma production is nonzero, but the chirality averaged with many events vanishes. In a word, there is only event-by-event  $P$  and  $CP$  violation in this case. To facilitate the study involving the asymmetry between left- and right-handed quarks, a chiral chemical

potential  $\mu_5$  is introduced, and the following term should be added to the Lagrangian density [8]

$$\mu_5 \bar{\Psi} \gamma_4 \gamma_5 \Psi. \quad (3)$$

As the introduction of a baryon chemical potential  $\mu$  would induce a net baryon density  $n$ , the chiral chemical potential  $\mu_5$  can induce the chirality density

$$n_5 = -N_c N_f \int \frac{d^4p}{(2\pi)^4} \text{tr}[S(p, \mu_5) \gamma_4 \gamma_5], \quad (4)$$

in which  $S$  is the quark propagator;  $N_c$  and  $N_f$  denote the color factor and the number of flavors, respectively; and the trace is taken over Dirac indices.

It is generally accepted that the chiral phase transition of QCD at low temperature and high baryon chemical potential is of first order and the first-order phase transition line terminates at the critical endpoint (CEP) [9–17]. Detecting the CEP has been one of the most important aims of worldwide experiments in high-energy heavy ion colliders. Locating its position and plotting the phase diagram is also a hot topic in the field of nonperturbative QCD. As previously discussed, the chiral imbalance might appear in the production of quark-gluon plasma event by event, so it is of interest to study the effect of this asymmetry on the phase diagram and on the position of the CEP. In the literature, the phase diagram with zero baryon density in the  $\mu_5 - T$  plane has been plotted out with the Polyakov–Nambu–Jona-Lasinio (PNJL) model,

\*wangbinphys@hust.edu.cn

†zonghs@nju.edu.cn

the linear sigma model coupled to quarks and to the Polyakov loop (PLSM<sub>q</sub>), and lattice QCD [18–21]; also, the phase diagram at  $T - \mu - \mu_5$  space is given by the PNJL model [22]. As the theory at finite  $\mu_5$  does not suffer from the sign problem [8], it is expected that the study in the  $\mu_5 - T$  plane using lattice QCD could provide useful information for the understanding of the phase structure in the  $\mu - T$  plane [20,22]. The Dyson–Schwinger equations (DSEs) are a widely adopted continuum nonperturbative field-theoretical method that has been proven to be successful in the study of chiral phase transition and hadron physics [23–25]. Compared to the Nambu–Jona-Lasinio model and some other chiral models, it can describe simultaneously the two most important low-energy phenomena of QCD, i.e., the dynamical chiral symmetry breaking and confinement. In this paper, we will study the previously discussed problems in the framework of the DSEs.

## II. THEORETICAL AND NUMERICAL ANALYSIS

It has been proven that the inverse of the quark propagator can include at most the following eight Lorentz structure components:  $\vec{\gamma} \cdot \vec{p}$ ,  $\gamma_4$ ,  $1$ ,  $\vec{\gamma} \cdot \vec{p}\gamma_4$ ,  $\vec{\gamma} \cdot \vec{p}\gamma_5$ ,  $\gamma_4\gamma_5$ ,  $\gamma_5$ ,  $\vec{\gamma} \cdot \vec{p}\gamma_4\gamma_5$  [26]. At finite temperature and/or baryon chemical potential but with no chiral imbalance, the most general form of the inverse of the quark propagator  $S^{-1}(\vec{p}_k)$  would include four Lorentz components [24,26],

$$S^{-1}(\vec{p}_k) = i\vec{\gamma} \cdot \vec{p}A(\vec{p}_k^2) - i\gamma_4\omega_k C(\vec{p}_k^2) + B(\vec{p}_k^2) + i\vec{\gamma} \cdot \vec{p}\gamma_4 D(\vec{p}_k^2), \quad (5)$$

in which  $\vec{q}_n = (\vec{q}, \tilde{\omega}_n)$ , with  $\tilde{\omega}_n = (2n+1)\pi T + i\mu$ . If the chiral chemical potential is nonzero, the chiral balance will be broken, and the Lorentz structure of the inverse of the quark propagator becomes

$$S^{-1}(\vec{p}_k, \mu_5) = i\vec{\gamma} \cdot \vec{p}A(\vec{p}_k^2, \mu_5) + i\gamma_4\omega_k C(\vec{p}_k^2, \mu_5) + B(\vec{p}_k^2, \mu_5) - i\vec{\gamma} \cdot \vec{p}\gamma_4 D(\vec{p}_k^2, \mu_5) + \gamma_5 G(\vec{p}_k^2, \mu_5) + \gamma_4\gamma_5 H(\vec{p}_k^2, \mu_5) + i\vec{\gamma} \cdot \vec{p}\gamma_5 E(\vec{p}_k^2, \mu_5) - i\vec{\gamma} \cdot \vec{p}\gamma_4\gamma_5 F(\vec{p}_k^2, \mu_5). \quad (6)$$

In the rainbow approximation, the gap equation can be written as

$$S^{-1}(\vec{p}_k, \mu_5) = S_0^{-1}(\vec{p}_k, \mu_5) + \frac{4}{3}T \sum_{n=-\infty}^{+\infty} \int \frac{d^3q}{(2\pi)^3} g^2 \times D_{\mu\nu}^{\text{eff}}(\vec{p}_k - \vec{q}_n, \mu_5) \gamma_\mu S(\vec{q}_n, \mu_5) \gamma_\nu, \quad (7)$$

in which  $S_0(\vec{p}_k, \mu_5)$  is the free quark propagator that can be derived from the Lagrangian,

$$S_0^{-1}(\vec{p}_k, \mu_5) = i\gamma_4\tilde{\omega}_k + i\vec{\gamma} \cdot \vec{p} + m - \mu_5\gamma_4\gamma_5. \quad (8)$$

In nowadays literature of the DSE, the effective model gluon propagator is often introduced as a physical input, and the quark propagator is calculated out by the gap equation with this input. There are two qualitative requirements for the effective gluon propagator in the DSE approach. First, the effective gluon propagator should simulate the infrared enhancement and confinement. Second, this gluon propagator should lead to dynamical chiral symmetry breaking, and the obtained quark propagator has no particlelike poles on the timelike  $p^2$  axis (so that quarks are confined). In other words, the physical input of the effective gluon propagator must ensure that the DSE has the features of confinement and dynamical chiral symmetry breaking simultaneously. The rank-2 confining separable model gluon propagator is a generally used effective model in the literature and was first proposed for describing the properties of light flavor pseudoscalar and vector mesons [27,28]. Simplicity is a big advantage of this model. It overcomes the difficulty in the summation of the frequency spectrum at finite temperature confronted in many other more sophisticated gluon propagator models [29–31], but it can be used to highlight many underlying mechanisms. In the literature, it has been used to study the chiral phase transition without considering the chiral imbalance and gives reasonable results compared to that obtained with other nonperturbative methods [9,10,32,33]. At finite temperature, chemical potential, and chiral chemical potential, this model gluon propagator can be written as

$$g^2 D_{\mu\nu}^{\text{eff}}(\vec{p}_k - \vec{q}_n, \mu_5) = \delta_{\mu\nu} [D_0 f_0(p_k^2) f_0(q_n^2) + D_1 f_1(p_k^2) p_k \cdot q_n f_1(q_n^2)], \quad (9)$$

in which  $\vec{q}_n = (\vec{q}, \tilde{\omega}_n)$ , with  $\tilde{\omega}_n = (2n+1)\pi T + i\mu$  [28,34,35],  $f_0(q_n^2) = \exp(-q_n^2/\Lambda^2)$ ,  $f_1(q_n^2) = \exp(-q_n^2/\Lambda_1^2)$ ,  $\Lambda_0 = 0.638$  GeV,  $\Lambda_1/\Lambda_0 = 1.21$ ,  $D_0\Lambda_0^2 = 260.0$ ,  $D_1\Lambda_1^4 = 130.0$ , and the degenerated light quark mass  $m = 5.3$  MeV [28]. As it is noted in Ref. [28], the UV cutoff of this model is much stronger than general asymptotic behavior, so it is not suitable to study the physics in which the asymptotic behavior becomes apparent but can be used in the study that centers on physics in the chiral symmetry broken phase and in the vicinity of the chiral phase transition.

Substituting Eqs. (8) and (9) into the gap equation (7), one obtains the coupled integral equations

$$A(\vec{p}_k^2, \mu_5) = 1 + a_1(T, \mu, \mu_5) f_1(p_k^2), \quad (10)$$

$$B(\vec{p}_k^2, \mu_5) = m + b_0(T, \mu, \mu_5) f_0(p_k^2) + b_1(T, \mu, \mu_5) \omega_k f_1(p_k^2), \quad (11)$$

$$C(\tilde{p}_k^2, \mu_5) = 1 + c_0(T, \mu, \mu_5) f_0(p_k^2) / \tilde{\omega}_k + c_1(T, \mu, \mu_5) f_1(p_k^2) \omega_k / \tilde{\omega}_k, \quad (12)$$

$$D(\tilde{p}_k^2, \mu_5) = F(\tilde{p}_k^2) = 0, \quad (13)$$

$$E(\tilde{p}_k^2, \mu_5) = e_1(T, \mu, \mu_5) f_1(p_k^2), \quad (14)$$

$$G(\tilde{p}_k^2, \mu_5) = g_0(T, \mu, \mu_5) f_0(p_k^2) + g_1(T, \mu, \mu_5) \omega_k f_1(p_k^2), \quad (15)$$

$$H(\tilde{p}_k^2, \mu_5) = -\mu_5 + h_0(T, \mu, \mu_5) f_0(p_k^2) + h_1(T, \mu, \mu_5) \omega_k f_1(p_k^2), \quad (16)$$

in which

$$a_1(T, \mu, \mu_5) = \frac{8}{3} \int_1 \tilde{q}^2 f_1(q_n^2) \frac{A(\tilde{q}_n^2, \mu_5) t_1 + H(\tilde{q}_n^2, \mu_5) t_2}{t_3}, \quad (17)$$

$$b_0(T, \mu, \mu_5) = \frac{16}{3} \int_0 f_0(q_n^2) \frac{B(\tilde{q}_n^2, \mu_5) t_1 + \tilde{q}^2 F(\tilde{q}_n^2, \mu_5) t_2}{t_3}, \quad (18)$$

$$b_1(T, \mu, \mu_5) = \frac{16}{3} \int_1 \omega_n f_1(q_n^2) \frac{B(\tilde{q}_n^2, \mu_5) t_1 + \tilde{q}^2 F(\tilde{q}_n^2, \mu_5) t_2}{t_3}, \quad (19)$$

$$c_0(T, \mu, \mu_5) = \frac{8}{3} \int_0 f_0(q_n^2) \frac{\tilde{\omega}_n C(\tilde{q}_n^2, \mu_5) t_1 - i \tilde{q}^2 E(\tilde{q}_n^2, \mu_5) t_2}{t_3}, \quad (20)$$

$$c_1(T, \mu, \mu_5) = \frac{8}{3} \int_1 \omega_n f_1(q_n^2) \frac{\tilde{\omega}_n C(\tilde{q}_n^2, \mu_5) t_1 - i \tilde{q}^2 E(\tilde{q}_n^2, \mu_5) t_2}{t_3}, \quad (21)$$

$$e_1(T, \mu, \mu_5) = -\frac{8}{3} \int_1 \tilde{q}^2 f_1(q_n^2) \frac{E(\tilde{q}_n^2, \mu_5) t_1 + i \tilde{\omega}_n C(\tilde{q}_n^2, \mu_5) t_2}{t_3}, \quad (22)$$

$$g_0(T, \mu, \mu_5) = \frac{16}{3} \int_0 f_0(q_n^2) \frac{G(\tilde{q}_n^2, \mu_5) t_1 + \tilde{q}^2 D(\tilde{q}_n^2, \mu_5) t_2}{t_3}, \quad (23)$$

$$g_1(T, \mu, \mu_5) = \frac{16}{3} \int_1 \omega_n f_1(q_n^2) \frac{G(\tilde{q}_n^2, \mu_5) t_1 + \tilde{q}^2 D(\tilde{q}_n^2, \mu_5) t_2}{t_3}, \quad (24)$$

$$h_0(T, \mu, \mu_5) = -\frac{8}{3} \int_0 f_0(q_n^2) \frac{H(\tilde{q}_n^2, \mu_5) t_1 + \tilde{q}^2 A(\tilde{q}_n^2, \mu_5) t_2}{t_3}, \quad (25)$$

$$h_1(T, \mu, \mu_5) = -\frac{8}{3} \int_1 \omega_n f_1(q_n^2) \frac{H(\tilde{q}_n^2, \mu_5) t_1 + \tilde{q}^2 A(\tilde{q}_n^2, \mu_5) t_2}{t_3}, \quad (26)$$

where  $\int_0 = D_0 T \sum_{n=-\infty}^{+\infty} \int \frac{d^3 q}{(2\pi)^3}$ ,  $\int_1 = D_1 T \sum_{n=-\infty}^{+\infty} \int \frac{d^3 q}{(2\pi)^3}$ ,  $t_1 = B^2 + \tilde{q}^2 (F^2 - D^2 - E^2 + A^2) - G^2 + \tilde{\omega}_n C^2 + H^2$ ,  $t_2 = -2(BF - DG - i \tilde{\omega}_n CE + AH)$ , and  $t_3 = t_1^2 - \tilde{q}^2 t_2^2$ .

By solving Eqs. (11)–(27) numerically, we can determine the phase diagram in the  $T - \mu - \mu_5$  space. The chiral phase transition lines in the  $T - \mu$  plane corresponding to different chiral chemical potentials  $\mu_5$  are plotted out in Fig. 1. The black point in each line is the CEP. It connects the crossover line (the dashed line) and the first-order phase transition line (the solid line). When the baryon chemical potential  $\mu$  is zero, the corresponding chiral phase transition line in the  $T - \mu_5$  plane is also plotted out (the long-dashed line). In Fig. 2, we plot the phase diagram for  $\mu_5 = 0$  and the trail of the CEP for  $\mu_5$  increasing from 0 MeV to 750 MeV in the  $T - \mu$  plane. It can be seen that the effect of  $\mu_5$  is somewhat different from the existing chiral model calculations; namely, the CEP first moves roughly along the phase boundary of the  $T - \mu$  plane in the smaller  $\mu$  direction, as in the chiral model calculations [20], but turns in the opposite direction to move away from the small chemical potential region, which is quite different than the existing studies and has apparent consistency with lattice

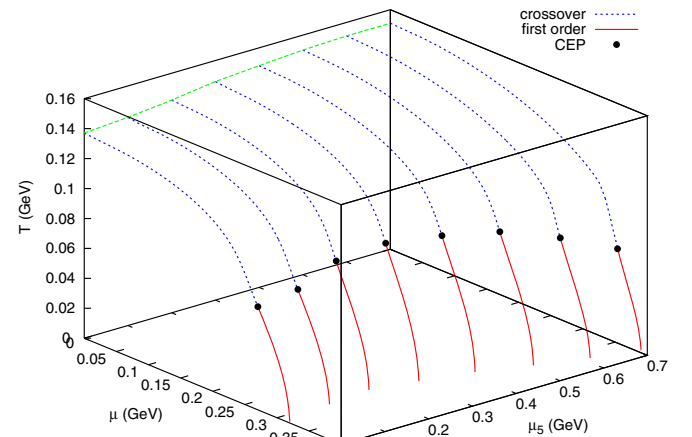


FIG. 1 (color online). The 3D phase diagram. For  $\mu_5$  increasing by each 100 MeV from 0 MeV, the corresponding chiral phase transition line in the  $T - \mu$  plane is plotted out. The black point in each line is the CEP. It connects the crossover line (the dashed line) and the first-order phase transition line (the solid line). When the baryon chemical potential  $\mu$  is zero, the corresponding chiral phase transition line in the  $T - \mu_5$  plane is also plotted out (the long-dashed line).

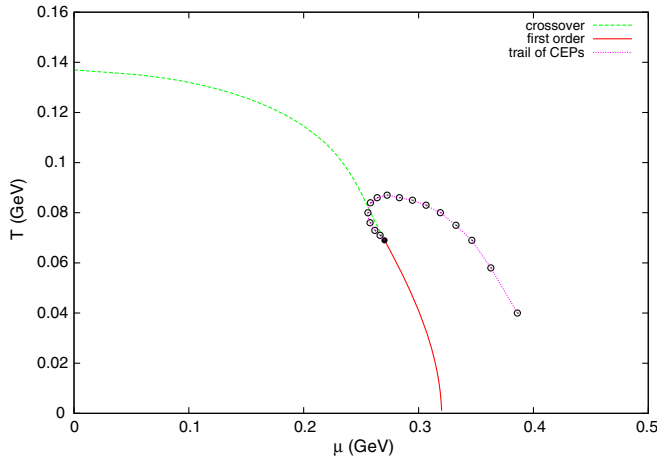


FIG. 2 (color online). The chiral phase diagram for  $\mu_5 = 0$  MeV and the trail of the CEPs in the  $\mu - T$  plane along with the variation of  $\mu_5$ . The black point is the CEP for  $\mu_5 = 0$  MeV. As the chiral chemical potential increases by each 50 MeV, the corresponding CEP is marked out by an open circle.

QCD calculation [21], which is to say the “CEP<sub>5</sub>” in the  $T - \mu_5$  plane might not exist. Our results also imply that, even if we include a small baryon chemical potential in the lattice QCD calculation, the CEP<sub>5</sub> might not be found, either. The black point that lies at  $(T_{\text{CEP}}^0, \mu_{\text{CEP}}^0) = (69 \text{ MeV}, 270.3 \text{ MeV})$  is the CEP for  $\mu_5 = 0$ . As the chiral chemical potential increases by each 50 MeV, the corresponding CEP is marked out by an open circle. It is shown that the position of the CEP moves almost in parallel with the crossover line to smaller baryon chemical potential when  $\mu_5 < 190$  MeV, and the CEP with the smallest  $\mu_{\text{CEP}}^* = 255.3$  MeV is obtained when  $\mu_5 = 190$  MeV, but when  $\mu_5 > 190$  MeV, the CEP moves toward a larger baryon chemical potential. It moves toward a high temperature when  $\mu_5 < 350$  MeV but moves toward a low temperature when  $\mu_5 > 350$  MeV. It will reach about  $0.58T_{\text{CEP}}^0$  when  $\mu_5 = 750$  MeV, at which temperature the chiral imbalance might hardly exist. In the literature, the phase diagram in the  $T - \mu_5$  plane with zero baryon number density has been plotted out using the PNJL model and PLSM<sub>q</sub>, which indicates that the chiral phase transition will be strengthened from a crossover to a first-order phase transition as the chiral chemical potential increases. But according to the trail of CEPs in Fig. 2, the chiral phase transition at finite temperature and chiral chemical potential but with zero baryon chemical potential should remain as a crossover, no matter how large the chiral chemical potential is (see the long-dashed line in the  $T - \mu_5$  plane in Fig. 1 and the top line in Fig. 6). In fact, this will always be the case for  $\mu < \mu_{\text{CEP}}^*$ . Our result indicates that the result obtained at finite  $(T, \mu_5)$  might not provide much useful information for the one at finite  $(T, \mu)$ . Furthermore, our result also indicates that, even with small baryon chemical potential under which condition lattice QCD calculation has no sign

problem, one still cannot find the CEP in the  $T - \mu_5$  plane. From the trail of the CEPs projected on the  $\mu - \mu_5$  plane (Fig. 3), it can also be found that  $\mu$  and  $\mu_5$  play definitely different roles in the chiral phase transition, so the result obtained in the  $T - \mu_5$  plane for zero or small values of  $\mu$  might not offer much help to the chiral phase transition at finite  $T$  and  $\mu$ . For  $\mu_{\text{CEP}}^* < \mu < \mu_{\text{CEP}}^0$ , the chiral phase transition will be strengthened from a crossover to a first-order phase transition as  $\mu_5$  increases, but it will be back to a crossover when  $\mu_5$  is large enough. For  $\mu > \mu_{\text{CEP}}^0$ , the chiral phase transition remains a first-order phase transition when  $\mu_5$  is small, but it will be weakened to a crossover when  $\mu_5$  is too large. The connection point of the crossover line and the first-order phase transition line is a CEP that indicates a second-order phase transition. We take  $\mu = 253.5, 265$ , and  $273$  MeV as the representative values for these three domains and will show the properties of them in detail below.

It is considered that the  $B$  function [in the quark propagator, Eq. (6)] evaluated at the lowest Matsubara frequency and zero momentum is an equivalent order parameter as the quark condensate, because it can completely determine the character of the chiral phase transition [36–38]. In this paper, we will adopt this definition:

$$\chi(T, \mu, \mu_5) = B(0, \tilde{\omega}_0^2, \mu_5). \quad (27)$$

The dependence of  $\chi(T, \mu, \mu_5)$  on  $T$  for  $\mu_5$  equal to 50, 100, and 500 MeV is plotted in Fig. 4. In each panel, the solid, long-dashed, and dashed lines represent that for  $\mu$  at 253.5, 265, and 273 MeV, respectively. When the baryon chemical potential is at 253.5 MeV (solid line), the chiral phase transition is always a crossover at all of the three axial chemical potentials. When the baryon chemical potential is at 265 MeV (long-dashed line), the chiral phase transition is of first order when the chiral chemical potential is at 100 MeV, but it is a crossover in other two cases. When

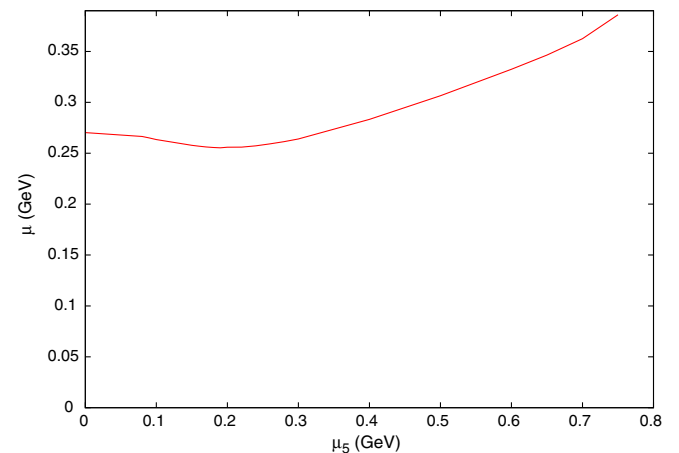


FIG. 3 (color online). The trail of the CEPs projected on the  $\mu - \mu_5$  plane.

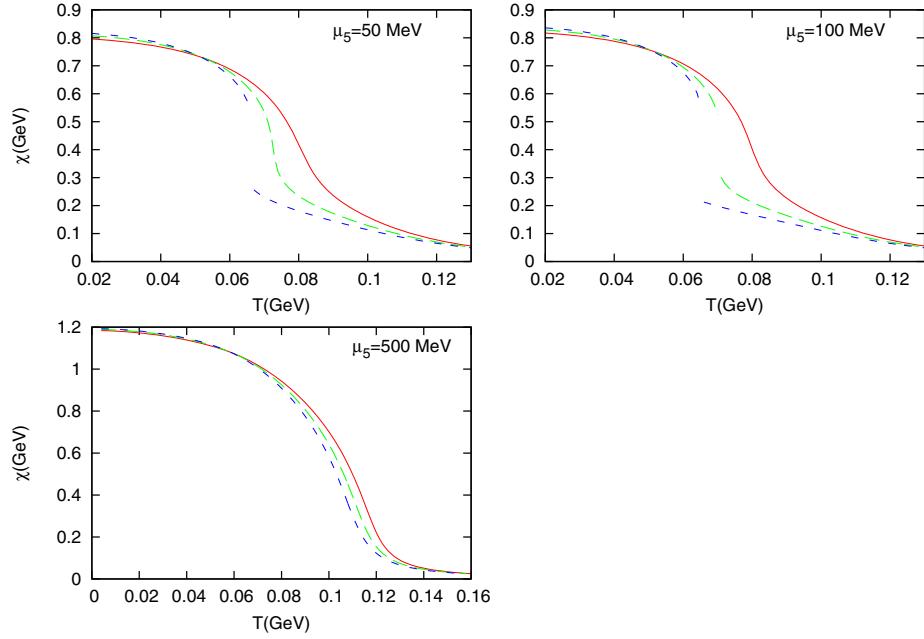


FIG. 4 (color online). The dependence of  $\chi(T, \mu, \mu_5)$  on  $T$  for  $\mu_5$  equal to 50 (the upper left panel), 100 (the upper right panel), and 500 MeV (the bottom left panel). In each panel, the solid, long-dashed, and dashed lines represent that for  $\mu$  at 253.5, 265, and 273 MeV, respectively.

the baryon chemical potential is at 273 MeV (dashed line), the chiral phase transition is of first order when the chiral chemical potential is at 50 and 100 MeV, but it is a crossover in the remaining case. From the variation of the chiral charge density  $n_5$  along with the temperature, we can find the same properties. The lines of  $n_5$  are plotted in Fig. 5 for the same  $\mu$

and  $\mu_5$  presented in the previous figure. In each panel, the first, second, and third lines (from top to bottom) represent that for  $\mu$  at 253.5, 265, and 273 MeV, respectively. It can be found that the chiral charge density will have an apparent step at the first-order chiral phase transition point but will change smoothly otherwise.

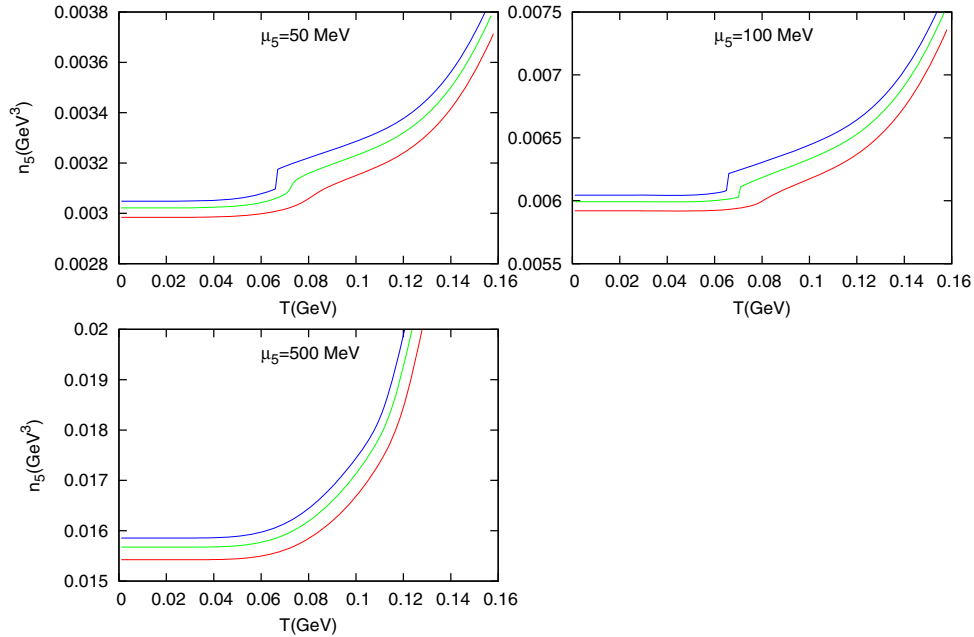


FIG. 5 (color online). The dependence of  $n_5(T, \mu, \mu_5)$  on  $T$  for  $\mu_5$  equal to 50 (the upper left panel), 100 (the upper right panel), and 500 MeV (the down left panel). In each panel, the first, second, and third lines (from top to bottom) represents that for  $\mu$  at 273, 265, and 253.5 MeV, respectively.

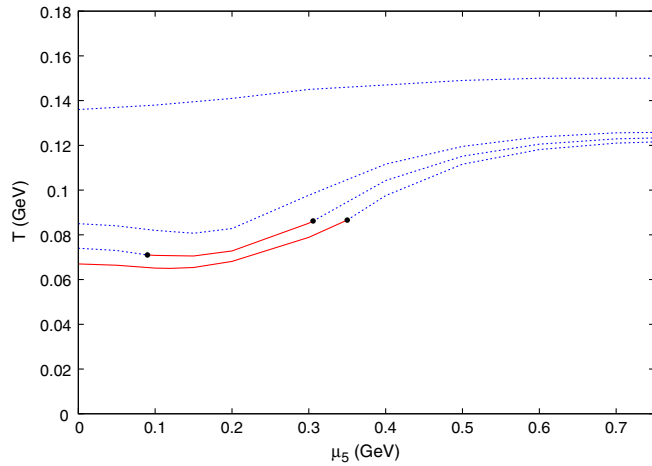


FIG. 6 (color online). The phase diagram in the  $T - \mu_5$  plane when  $\mu$  is at 0, 253.5, 265, and 273 MeV (from top to bottom). The solid line represents the first-order phase transition, while the dashed line represents the crossover.

In fact, as we previously discussed, for  $\mu = 253.5$  MeV, which is smaller than  $\mu_{\text{CEP}}^*$ , the chiral phase transition will always be a crossover in the  $T - \mu_5$  plane. For  $\mu = 265$  MeV, the chiral phase transition is a crossover when  $\mu_5 < 90$  MeV, but it will be strengthened to a first-order phase transition when  $90 \text{ MeV} < \mu_5 < 305.5$  MeV and will be back to a crossover when  $\mu_5 > 305.5$  MeV. For  $\mu = 273$  MeV, the chiral phase transition is of first order when  $\mu_5 < 350$  MeV, but it will be weakened to a crossover when  $\mu_5 > 350$  MeV. The corresponding phase diagram in the  $T - \mu_5$  plane is plotted in Fig. 6. Then, let us look again at the chiral phase transition line when  $\mu = 265$  MeV. Its first-order part would become shorter and shorter as  $\mu$  increases toward  $\mu_{\text{CEP}}^0$  and at last shrink to be a CEP point when  $\mu$  is equal to  $\mu_{\text{CEP}}^0$ . But its first-order part would become longer and longer as  $\mu$  decreases toward  $\mu_{\text{CEP}}^*$ , and its left CEP point will reach the temperature axis when  $\mu$  is equal to  $\mu_{\text{CEP}}^*$ .

As discussed above, our results have apparent consistency with the lattice QCD result [21], but they are quite different in the chiral model calculations [20]. A natural question that would arise is the following: are these results artifacts or in some sense physical? To study this further, we have also been trying to use some more elegant as well as widely used gluon models (which means more reliable conclusions), such as the famous Maris–Tandy model [39]. The numerical calculations are then much more difficult than the separable model, but the preliminary results show that the qualitative behaviors are similar; namely, at some critical  $\mu_5$  and larger values,  $\mu_c$  of the CEP will turn back to increase instead of decrease [40].

### III. CONCLUSIONS

In this paper, we study the effect of chiral imbalance on the chiral phase transition diagram, especially on the

positions of the CEP, in the framework of Dyson–Schwinger equations. Our result indicates that the CEP will move toward the temperature axis almost in parallel with the crossover line when  $\mu_5$  increases from 0 to 190 MeV, but it will move backward to bigger  $\mu$  when  $\mu_5 > 190$  MeV. The chiral phase diagram in the  $T - \mu_5$  plane for  $\mu$  at different values is studied. It is found that the corresponding chiral phase diagram on this plane is a crossover when the baryon chemical potential is zero and will always be the case when  $\mu$  is smaller than  $\mu_{\text{CEP}}^*$ . Together with the trail of CEPs projected on the  $\mu - \mu_5$  plane, we conclude that  $\mu$  and  $\mu_5$  have no similarity in the chiral phase transition, and we cannot expect the study in the  $T - \mu_5$  plane (with  $\mu$  equal to zero or a small value) can provide much useful information for the study at finite  $T$  and  $\mu$  (without chiral chemical potential). These results are different from that obtained using the PNJL model and PLSM<sub>q</sub> [18–20,22]. But lattice QCD calculation without baryon chemical potential does not find the CEP<sub>5</sub> in the  $T - \mu_5$  plane [21]. We expect that, even if one includes a small baryon chemical potential in the lattice QCD calculation, the CEP<sub>5</sub> might not be found, either. Although the trail of CEPs in this paper is different from that obtained from the PNJL model and PLSM<sub>q</sub> [18–20,22], at small chiral chemical potential, both our work and those works have the same result that the CEP moves toward the temperature axis when  $\mu_5$  increases (here, we note that, although Refs. [18,19,22] do not consider the baryon chemical potential, from its phase diagram in the  $T - \mu_5$  plane, we can deduce that the CEP should move toward the temperature axis as  $\mu_5$  increases). Since the chiral condensate is not very small in the neighborhood of the CEP<sub>5</sub> and the chiral condensate can suppress the chirality,  $\mu_5$  in this region might not be very large. So the most probable phenomenon observed in experiments is that the CEP is pushed farther from the temperature axis by chiral imbalance. And to some extent, our results, which have apparent consistency with the lattice calculation, indicate that the physics related to the chiral chemical potential deserve further studies. Some further discussions with more elegant gluon models, which means more reliable conclusions, are in the works [40]. Last but not least, we need to say that to identify the origin of the discrepancy between our work and the previous chiral models is necessary and important. A possible reason for this discrepancy may be the cutoff artifact, and this is also one of our future works.

### ACKNOWLEDGMENTS

This work is supported in part by the National Natural Science Foundation of China (under Grants No. 11275097 and No. 11475085), the National Basic Research Program of China (under Grant No. 2012CB921504), and the Jiangsu Planned Projects for Postdoctoral Research Funds (under Grant No. 1402006C).

- [1] A. A. Belavin, A. M. Polyakov, A. S. Shvarts, and Yu. S. Tyupkin, *Phys. Lett.* **59B**, 85 (1975).
- [2] G. 't Hooft, *Phys. Rev. Lett.* **37**, 8 (1976); *Phys. Rev. D* **14**, 3432 (1976).
- [3] L. McLerran, E. Mottola, and M. E. Shaposhnikov, *Phys. Rev. D* **43**, 2027 (1991).
- [4] G. D. Moore, *Phys. Lett. B* **412**, 359 (1997); G. D. Moore and K. Rummukainen, *Phys. Rev. D* **61**, 105008 (2000); D. Bödeker, G. D. Moore, and K. Rummukainen, *Phys. Rev. D* **61**, 056003 (2000); G. D. Moore, arXiv:hep-ph/0009161.
- [5] S. L. Adler, *Phys. Rev.* **177**, 2426 (1969); J. S. Bell and R. Jackiw, *Nuovo Cimento A* **60**, 47 (1969).
- [6] N. H. Christ, *Phys. Rev. D* **21**, 1591 (1980).
- [7] A. V. Smilga, *Phys. Rev. D* **45**, 1378 (1992).
- [8] K. Fukushima, D. E. Kharzeev, and H. J. Warringa, *Phys. Rev. D* **78**, 074033 (2008).
- [9] B. Wang, W. M. Sun, and H. S. Zong, *Mod. Phys. Lett. A* **28**, 1350064 (2013).
- [10] B. Wang, Z. F. Cui, W. M. Sun, and H. S. Zong, *Few-Body Syst.* **55**, 47 (2014).
- [11] Y. Aoki, Z. Fodor, S. D. Katz, and K. K. Szabó, *Phys. Lett. B* **643**, 46 (2006).
- [12] F. Karsch, *Proc. Sci.*, CPOD07 (2007) 126.
- [13] O. Philipsen, *Eur. Phys. J. Spec. Top.* **152**, 29 (2007).
- [14] M. Stephanov, *Prog. Theor. Phys. Suppl.* **153**, 139 (2004); [*Int. J. Mod. Phys. A* **20**, 4387 (2005)].
- [15] Z. F. Cui, C. Shi, Y. H. Xia, Y. Jiang, and H. S. Zong, *Eur. Phys. J. C* **73**, 2612 (2013).
- [16] Y. Jiang, H. Chen, W. M. Sun, and H. S. Zong, *J. High Energy Phys.* **04** (2013) 014.
- [17] C. Shi, Y. L. Wang, Y. Jiang, Z. F. Cui, and H. S. Zong, *J. High Energy Phys.* **07** (2014) 014.
- [18] K. Fukushima, M. Ruggieri, and R. Gatto, *Phys. Rev. D* **81**, 114031 (2010).
- [19] M. N. Chernodub and A. S. Nedelin, *Phys. Rev. D* **83**, 105008 (2011).
- [20] M. Ruggieri, *Phys. Rev. D* **84**, 014011 (2011).
- [21] A. Yamamoto, *Phys. Rev. Lett.* **107**, 031601 (2011).
- [22] R. Gatto and M. Ruggieri, *Phys. Rev. D* **85**, 054013 (2012).
- [23] C. D. Roberts and A. G. Williams, *Prog. Part. Nucl. Phys.* **33**, 477 (1994).
- [24] C. D. Roberts and S. M. Schmidt, *Prog. Part. Nucl. Phys.* **45**, S1 (2000).
- [25] I. C. Cloët and C. D. Roberts, *Prog. Part. Nucl. Phys.* **77**, 1 (2014).
- [26] O. K. Kalashnikov, *Pis'ma Zh. Eksp. Teor. Fiz.* **41**, 477 (1985) [*JETP Lett.* **41**, 582 (1985)].
- [27] C. J. Burden, L. Qian, C. D. Roberts, P. C. Tandy, and M. J. Thomson, *Phys. Rev. C* **55**, 2649 (1997).
- [28] D. Blaschke, G. Bureau, Yu. L. Kalinovsky, P. Maris, and P. C. Tandy, *Int. J. Mod. Phys. A* **16**, 2267 (2001).
- [29] P. Maris and C. D. Roberts, *Phys. Rev. C* **56**, 3369 (1997).
- [30] P. Maris and P. C. Tandy, *Phys. Rev. C* **61**, 045202 (2000).
- [31] S. X. Qin, L. Chang, Y. X. Liu, C. D. Roberts, and D. J. Wilson, *Phys. Rev. C* **84**, 042202 (2011).
- [32] M. He, J. F. Li, W. M. Sun, and H. S. Zong, *Phys. Rev. D* **79**, 036001 (2009).
- [33] M. He, F. Hu, W. M. Sun, and H. S. Zong, *Phys. Lett. B* **675**, 32 (2009).
- [34] D. Blaschke and P. C. Tandy, *International Workshop on Understanding Deconfinement in QCD, Trento, Italy, 1999* (World Scientific, Singapore, 2000), p. 218, <http://arxiv.org/abs/nucl-th/9905067v1>.
- [35] D. Blaschke and C. D. Roberts, *Nucl. Phys.* **A642**, c197 (1998).
- [36] D. Blaschke, A. Höll, C. D. Roberts, and S. Schmidt, *Phys. Rev. C* **58**, 1758 (1998).
- [37] A. Höll, P. Maris, and C. D. Roberts, *Phys. Rev. C* **59**, 1751 (1999).
- [38] A. D. Jackson and J. J. M. Verbaarschot, *Phys. Rev. D* **53**, 7223 (1996).
- [39] P. Maris and P. C. Tandy, *Phys. Rev. C* **60**, 055214 (1999).
- [40] S. S. Xu, Z. F. Cui, B. Wang, Y. M. Shi, Y. C. Yang, and H. S. Zong (unpublished).